

Coupled Electronic and Nuclear Motions during Azobenzene Photoisomerization Monitored by Ultrafast Electron Diffraction

Jérémy R. Rouxel,* Daniel Keefer,* Flavia Aleotti, Artur Nenov, Marco Garavelli, and Shaul Mukamel*



Cite This: <https://doi.org/10.1021/acs.jctc.1c00792>



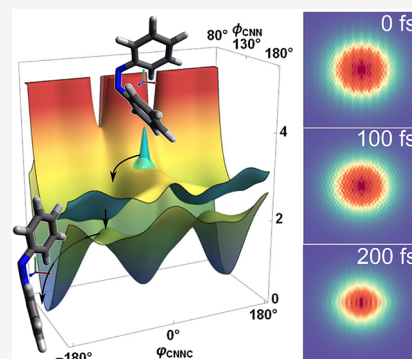
Read Online

ACCESS |

Metrics & More

Article Recommendations

ABSTRACT: Ultrafast electron diffraction is a powerful technique that can resolve molecular structures with femtosecond and angstrom resolutions. We demonstrate theoretically how it can be used to monitor conical intersection dynamics in molecules. Specific contributions to the signal are identified which vanish in the absence of vibronic coherence and offer a direct window into conical intersection paths. A special focus is on hybrid scattering from nuclei and electrons, a process that is unique to electron (rather than X-ray) diffraction and monitors the strongly coupled nuclear and electronic motions in the vicinity of conical intersections. An application is made to the cis to trans isomerization of azobenzene, computed with exact quantum dynamics wavepacket propagation in a reactive two-dimensional nuclear space.



1. INTRODUCTION

Ultrafast electron diffraction (UED) is a well established technique that can resolve in space and time molecular structures as they undergo ultrafast dynamics.^{1,2} It can potentially be more sensitive than time-resolved X-ray diffraction (XRD) due to the stronger interaction between electrons and molecules compared to photons.³ Space charge effects have limited the atomic and temporal resolution required to follow ultrafast femtosecond dynamics.^{4,5} Additionally, low signal-to-noise ratios limit the ability to deconvolve the signal and the instrument response function, which is crucial for a high temporal resolution.^{5,6} An important effort has been recently directed at improving the temporal resolution of electron pulse sources using nonrelativistic⁷ or relativistic⁶ sources. Recent experiments are pushing the observable limits of dynamical pathways to the femtosecond regime.^{8–11}

Most UED studies have so far focused on resolving the evolving structure of electronically excited molecules undergoing photophysical and photochemical processes.¹² These have led to striking observations of electronic and nuclear relaxation. However, time-resolved homodyne-detected diffraction signals are not solely determined by the time dependent charge density but should be dissected into various contributions, each having a distinct physical significance.^{13,14} The UED pattern originates from both the electronic σ_E and the nuclear σ_N molecular charge densities. The UED signal from a single molecule is given by a two-point correlation function of the total (electronic + nuclear) charge density. As such, it contains purely electronic, purely nuclear, and hybrid

electronic and nuclear contributions. The purely electronic terms are the same as in XRD,^{15,16} up to a prefactor, and this component of the UED signals thus carries the same information as XRD. When this contribution is further expanded in molecular eigenstates, it is possible to single out terms sensitive to molecular coherences.^{13,17} The nuclear and hybrid terms, which do not appear in XRD, offer novel insights into the molecular dynamics and are highly sensitive to conical intersections (CoIns).

Azobenzene has two stable trans and cis isomers in the electronic ground state, see Figure 1. Its photoisomerization has drawn considerable interest for photoswitching application in materials,¹⁸ neurons¹⁹ and protein folding.²⁰ Selective optical switching between the two isomers with high quantum yield is possible by using different wavelengths. The isomerization is triggered by photoexcitation from the S_0 to the $n\pi^*$ S_1 state.^{21,22} High-level CASPT2 potential energy surfaces in the reduced space of three nuclear degrees of freedom describing the isomerization reaction were reported in ref 23. The first nuclear coordinate is the carbon–nitrogen–nitrogen–carbon (C–N–N–C) dihedral angle connecting the cis minimum at 5° with the trans minimum at 180° . The second and third coordinates are the two respective C–N–N bending

Received: August 6, 2021

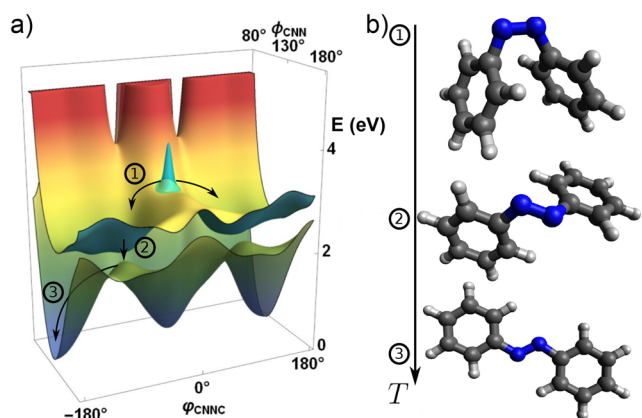


Figure 1. (a) The S_0 and S_1 potential energy surfaces of azobenzene. The wavepacket in ① is initially localized around the cis geometry in the S_1 state and moves toward the CoIn in ②. After crossing the CoIn, the wavepacket reaches the trans geometry within few hundreds femtoseconds. (b) Single point geometries of the cis ①, trans ③ isomers and at the CoIn ②.

angles between the two nitrogen atoms and one adjacent carbon atom, respectively. To simulate nuclear wavepacket

dynamics for the cis to trans isomerization, it is sufficient to include one of the two CNN angles, while the other one remains fixed at 116° .¹³ Symmetry breaking between both angles is necessary to reach the minimum energy conical intersection, that spans a strong nonadiabatic coupling seam between $\text{CNN} = 127^\circ$ and 152° . Hybrid pathways have been discussed and known as rotation-assisted inversion or inversion-assisted rotation. The isomerization dynamics time scale exhibits a multiexponential decay with time scales ranging from ≈ 0.2 ps to ≈ 12 ps²⁴ for the dynamics in the S_1 state. In Figure 2, the nuclear wavepacket amplitude squared is displayed as a function of the torsion and bending angles for different time delays (0, 100, and 200 fs). The average molecular geometry is displayed for each of these three times.

In section 2, we first summarize how the UED signal can be dissected into multiple interaction pathways. Next, we present how the various contributions to the signal, that is, elastic/inelastic and electronic/nuclear contributions, offer different windows into the ultrafast isomerization dynamics. In section 3, we discuss how these contributions can be discriminated experimentally.

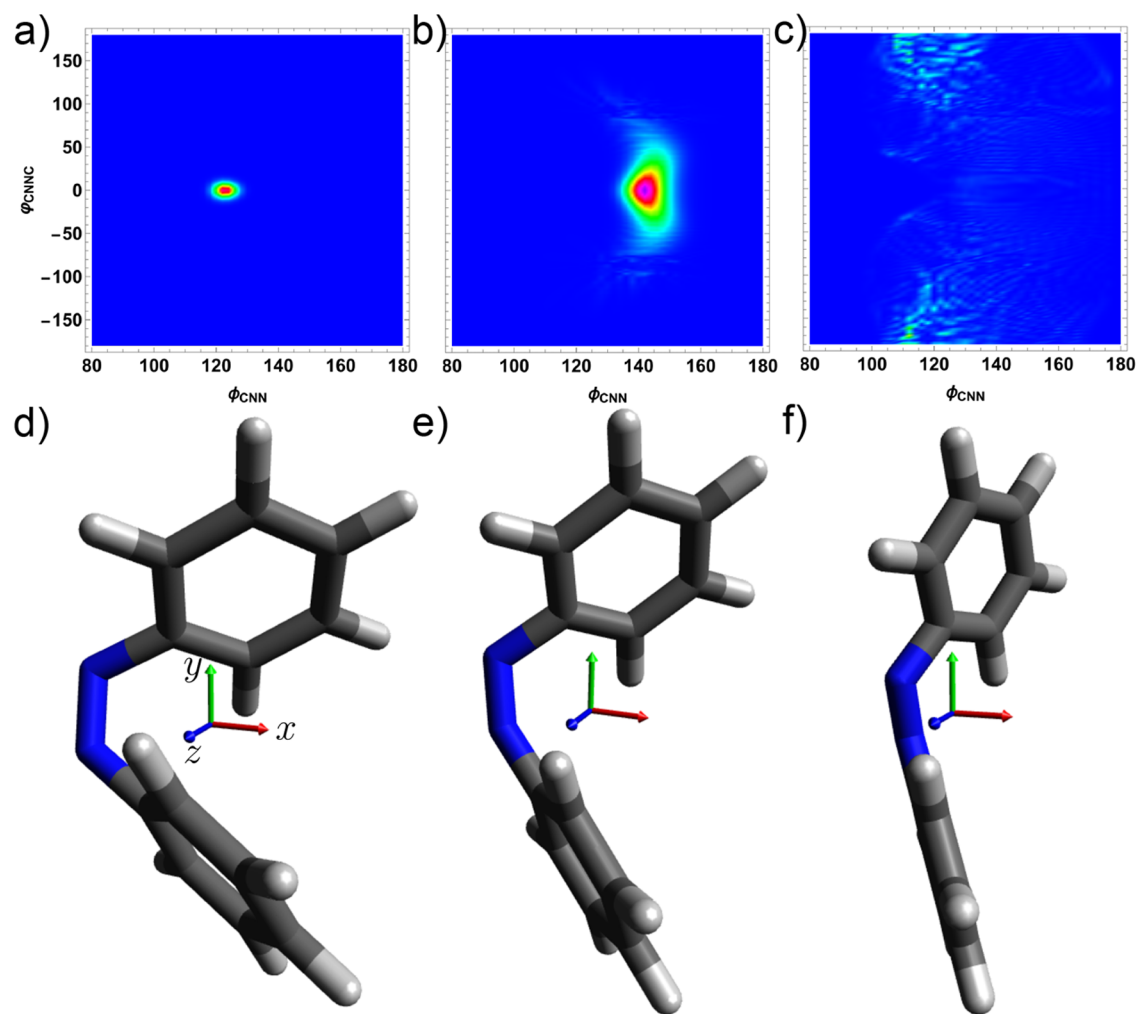


Figure 2. Amplitude squared of the excited state wavepacket at $T = 0, 100,$ and 200 fs in panels a, b, and c, respectively. Panels d, e, and f show the corresponding averaged molecular geometries at the same time delays.

2. RESULTS

The UED Signals. The UED signal defined in the [Materials and Methods](#) section is given by¹⁴

$$S_{\text{UED}}(\mathbf{q}, T) = \frac{2}{\epsilon_0^2 \hbar^2 q^4} \Re \int dt dt' \langle \sigma_{\text{T}}(-\mathbf{q}, t) \sigma_{\text{T}}(\mathbf{q}, t') \rangle \times F_e(t) F_e^*(t') e^{i\omega_e(t-t')} \quad (1)$$

where $\mathbf{q} = \mathbf{k}_s - \mathbf{k}_e$ is the momentum transfer between the scattered and incoming electron beams with wavevectors \mathbf{k}_s and \mathbf{k}_e , respectively. $\sigma_{\text{T}} = \sigma_{\text{E}} + \sigma_{\text{N}}$ is the total charge density given by the sum of the unscreened electronic σ_{E} and nuclear σ_{N} charge densities. F_e is the electron beam temporal envelope. Equation 1 can be further simplified by assuming that (1) no field is initially present in the detector direction (homodyne detection), (2) the signal originates from a single molecule, (3) the electron pulse is impulsive $F_e(t) \propto \delta(t - T)$. Under these conditions, eq 1 becomes

$$S_{\text{UED}}(\mathbf{q}, T) \propto \frac{1}{q^4} \langle \Psi(T) | \sigma_{\text{T}}(-\mathbf{q}) \sigma_{\text{T}}(\mathbf{q}) | \Psi(T) \rangle \quad (2)$$

The electrons + nuclei wave function $|\Psi(T)\rangle = \sum_i |\chi_i(T)\rangle |\varphi_i\rangle$ is expanded in the adiabatic basis set consisting of products of nuclear $|\chi_i(T)\rangle$ and electronic $|\varphi_i\rangle$ many-body states in state i . T is the delay between the initial actinic pulse launching the dynamics and the electron beam scattering event.

These expressions have close similarities with the tr-XRD signal¹³ but with some notable differences: XRD only involves the electronic charge density while UED depends on the total electronic + nuclear charge density. In addition, the $1/q^4$ prefactor dampens the high q contributions. By expanding the two-point correlation function in eq 2 in the valence electronic states, the 12 contributions to the UED signal can be expressed by the loop diagrams, given in Figure 8 in the [Materials and Methods](#) section.

$$S_{\text{UED}}(\mathbf{q}, T) \propto \sum_{i=1}^{12} S_{\text{UED}}^{\text{Di}}(\mathbf{q}, T) \quad (3)$$

Application to the Cis–Trans Isomerization of Azobenzene. All 12 contributions to the UED signal¹⁴ were calculated for oriented azobenzene molecules. The fixed laboratory frame is displayed in panels d, e, and f of Figure 2. The potential energy surfaces (PES) of the S_0 and the S_1 states, see Figure 1 were computed by ab initio quantum chemistry using RASSCF and RASPT2 modules with MOLCAS.²⁵ The wavepacket propagation was simulated by solving the time-dependent Schrödinger equation numerically in the reduced two-dimensional space spanned by the CNN bond angle and the CNNC dihedral angle. Details are given in the methods section. Charge density matrix elements in the electronic space were computed on a numerical grid for the nuclear coordinates, and their products were averaged over the nuclear wavepacket to obtain the necessary charge density matrix elements for single molecule signals. Diagonal and off-diagonal matrix elements of the charge density operator averaged over the nuclear wavepacket are displayed in Figure 3.

The simulated UED signal, eq 3, is depicted in Figure 4. To eliminate the divergence at the origin, the signal has been multiplied by q^4 . At $T = 0$ fs, the excited nuclear wavepacket located in the S_1 state is represented by a Gaussian wavepacket centered at the cis geometry. It reaches the CoIn after 70 fs at the geometry $\textcircled{2}$ displayed in Figure 1. This assumes an

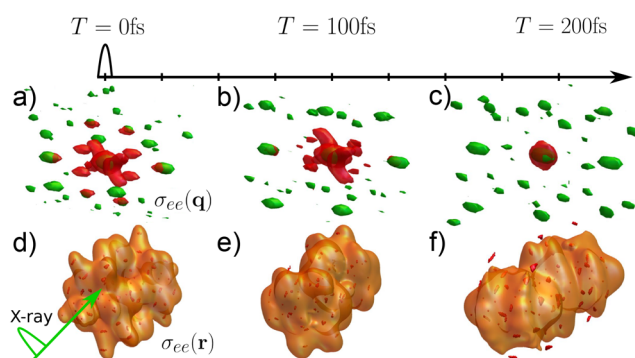


Figure 3. Charge densities at 0, 100, and 200 fs after the actinic excitation of cis-azobenzene. Panels a, b, and c display the Fourier transform of the charge densities measured in the UED experiment. The electronic and nuclear contributions are in red and green, respectively. Corresponding real space electronic (orange) and nuclear (red) charge densities of the e state are shown in panels d, e, and f.

excitation of 100% of the ground state into the S_1 state.²⁶ Experimental excitations are usually lower to keep the process in the linear regime and avoid multiphoton processes. A lower than 100% excitation adds a constant background from elastic ground state scattering to the signal. This only affects the relative strengths of the different signatures, but not the qualitative features. Scattering experiments and analysis with low excitation ratios (around 5%) have been demonstrated.²⁷

Figure 5 displays the electronic, nuclear and hybrid contributions to the UED signal in q – T space along the q_x , q_y , or q_z . The top row shows the total signal. The electronic contribution, diagrams (i) to (vi) in Figure 8, displayed in the second row, is the main contribution to the total signal and has already been studied previously for tr-XRD.¹⁵ A careful inspection shows some minor differences between the total signal and the electronic contribution, especially at short time and large q values where the nuclei contributions are visible. This signal displays a particular sensitivity to the CoIn. Along q_y , for example, the signal at $q_y = 5 \text{ \AA}^{-1}$ starts fading at $T = 70$ fs when the CoIn is being crossed, while another feature appears at $q_y = 8 \text{ \AA}^{-1}$. The second row shows the nuclear contributions to the signal, given by diagrams (vii) and (viii) in Figure 8. Initially, the nuclear wavepacket is well localized at the cis geometry and the atomic nuclear charges are centered around their atomic sites. This is why the nuclear signal is more delocalized in q space than its electronic counterpart at the beginning of the dynamics. As the nuclear wavepacket spreads, the electronic density at the atomic sites becomes more delocalized and the signals are dominated by the lower q values as shown in Figure 5. The nuclear contribution contains features at multiple q values that vanish when the CoIn is reached. The final hybrid electronic/nuclear terms are displayed at the bottom row of Figure 5. These are mostly located around low q values where both the electronic and nuclear charge densities overlap in q space. Along q_y , the signal contains a clear feature at 10 \AA^{-1} that appears at the onset of the CoIn at 70 fs and vanishes at 170 fs with the vanishing of the coherence between the S_0 and the S_1 state (Figure 3b). While the electronic contributions in the top row are observable with X-ray diffraction as well, the nuclear and hybrid terms in the middle and bottom rows are unique to UED.

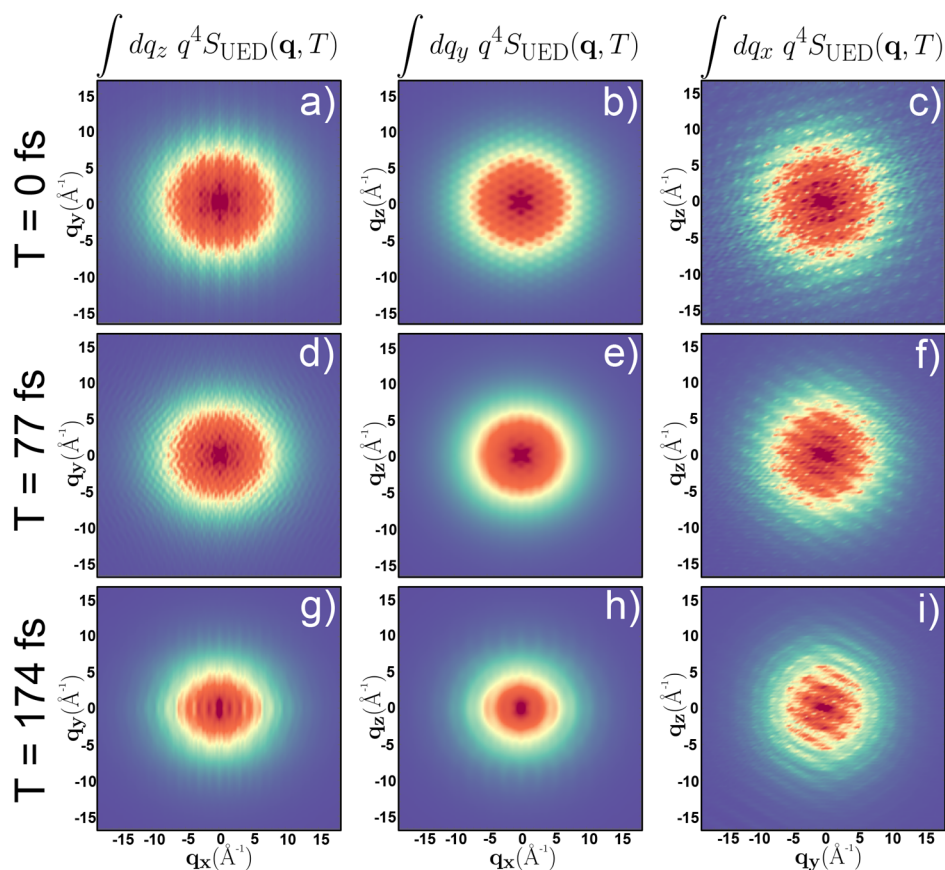


Figure 4. UED diffraction patterns at the initial time (top), at 80 fs when the CoIn is reached (middle), and at 170 fs (bottom) and for different projections in q space along q_z (a,d,g), q_y (b,e,h), and q_x (c,f,i).

A different partitioning of the 12 contributions to the signal is presented in Figure 6. The top row depicts the elastic contributions (diagrams (i), (ii), (vii), (viii), (ix), and (x), see Figure 8) whereas the bottom row displays the inelastic contributions to the signal ((iii), (iv), (v), (vi), (xi), and (xii)). The inelastic signal reveals the most direct information on the CoIn since it is induced by the coherence created as the CoIn is being crossed.

3. DISCUSSION

Each diagram contributing to the UED signals carries a distinct information regarding the molecular dynamics. The electronic (second row, Figure 5) and nuclear (third row, Figure 5) contributions to the signal measure Fourier transforms of the two-point correlation functions of the electronic and nuclear charge densities, respectively. Additionally, the hybrid electronic/nuclear terms (bottom row, Figure 5) possess unique features of the CoIns region. The hybrid contributions to UED in the q -values above 5 \AA^{-1} , zoomed in Figure 7 bottom panel, are very sensitive to the passage through the CoIn as can be compared with the dynamics of the coherence showed in Figure 7 top panel. The ability to extract them from the total signal would be an invaluable tool to study the dynamics. At conical intersections, the electrons and nuclei move on a comparable time scale and thus become strongly coupled. The hybrid nuclear/electronic term, that is unique to UED, is the most adequate one to observe this coupled motion.

The elastic terms contain products of diagonal matrix elements of the charge density operator that scale as the square of the number of electrons N^2 in the molecule. On the other hand, the inelastic terms have the scaling of a single valence electron and are therefore much weaker. Nonetheless, they can be separated by energy resolved detection since the scattered electron is shifted in energy by few electron-volts. Finally, by subtracting the different contributions to the frequency-resolved signal from the one without frequency resolution, one can recover the hybrid terms.

Since the electronic charge density is more delocalized than the nuclear one, its contribution to the diffraction pattern is limited to smaller momentum transfer values. At high q the signal is thus dominated by the nuclear terms. Separating the contributions at smaller q , up to few \AA^{-1} is a more delicate task which will require the use of information derived from other measurements.²⁸ The XRD diffraction pattern is produced by the electronic charge density. Similarly, neutron diffraction patterns solely originate from the nuclear charge density. By proper scaling, for example, following the Mott-Bethe formula for XRD,²⁹ one can subtract these contributions from the UED signal to single out the hybrid electronic/nuclear terms. The UED signal can be alternatively analyzed in combination with time-resolved photoelectron spectroscopy (TRPES) to extract additional energy information.³⁰

4. CONCLUSIONS

In this work, we have addressed the dissection of UED signals to extract the complete information on the electron and

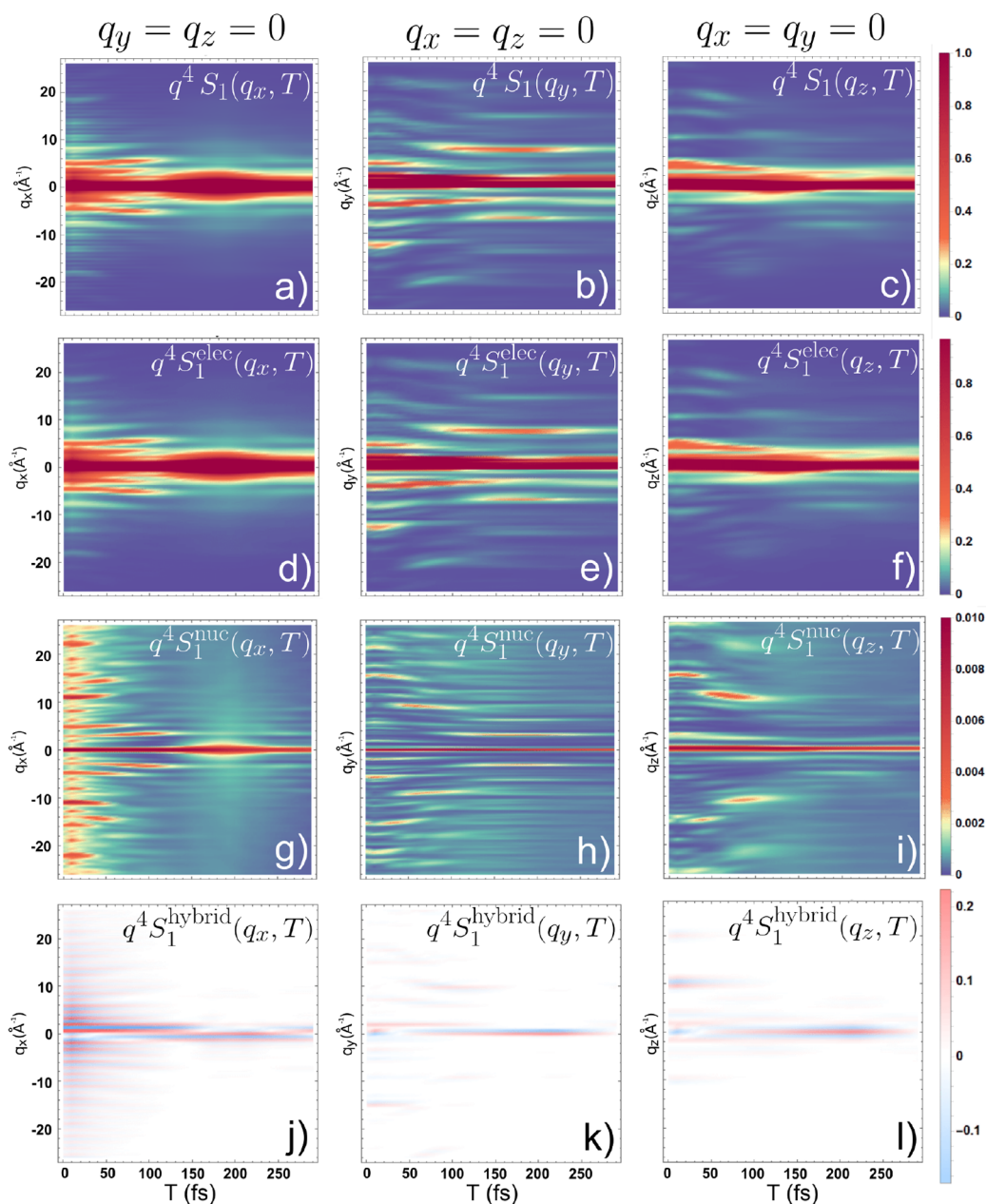


Figure 5. Total (a,b,c), electronic (d,e,f), nuclear (g,h,i), and hybrid (j,k,l) contributions to UED along q_x , q_y , and q_z from left to right. The electronic contribution is the sum of diagrams (i) to (vi) of the UED in Figure 8. The nuclear contribution is the sum of diagrams (vii) and (viii) and the hybrid electronic/nuclear contribution is the sum of diagrams (ix) to (xii).

nuclear molecular dynamics. A perturbative loop diagrams description reveals the existence hybrid electronic/nuclear terms in the signal. Although these terms are weaker than their purely electronic or nuclear counterparts, they display a high sensitivity to the nuclear dynamics, especially at conical intersections. Experimental efforts targeted at extracting these hybrid contributions should be valuable to gain detailed insight into nonadiabatic dynamics.

To highlight the features of the proposed signal, we have considered an idealized configuration in which the molecule was perfectly oriented. Also, the dynamics in the present study starts with a nuclear wavepacket fully in the excited state. A more realistic approach would assume an extra pump pulse and a partial population of the excited state. Future work should

consider the case of a complete or partial rotational averaging and include explicitly the pump pulse in the propagation.

Finally, we demonstrated that UED is sensitive to both electronic and nuclear dynamics, not only to structural changes. This point was also made recently by de Kock et al.³¹

5. MATERIALS AND METHODS

Signal Definitions. The molecule-beam interaction Hamiltonian for ultrafast ED is

$$H_{\text{int}}^{\text{UED}} = \int d\mathbf{r} d\mathbf{r}' \frac{\sigma_{\text{T}}(\mathbf{r})\sigma_{\text{B}}(\mathbf{r}')}{4\pi\epsilon_0|\mathbf{r} - \mathbf{r}'|} \quad (4)$$

where $\sigma_{\text{T}}(\mathbf{r}) = \sigma_{\text{E}}(\mathbf{r}) + \sigma_{\text{N}}(\mathbf{r})$ is the total molecular charge density operator (electron + nuclei) and $\sigma_{\text{B}}(\mathbf{r}')$ is the one of the incoming electron beam.

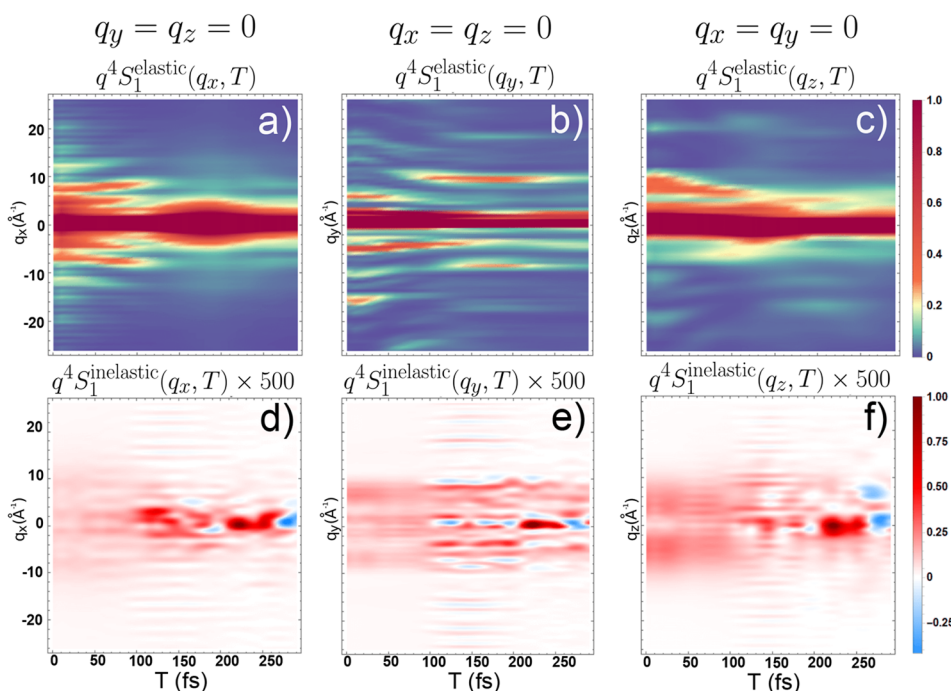


Figure 6. Elastic (a,b,c) and inelastic (d,e,f) contributions to UED. Top: Sum of the elastic contributions (diagrams (i), (ii), (vii), (viii), (ix), and (x) in Figure 8). Bottom: Sum of the inelastic contributions (diagrams (iii), (iv), (v), (vi), (xi), and (xii) in Figure 8).

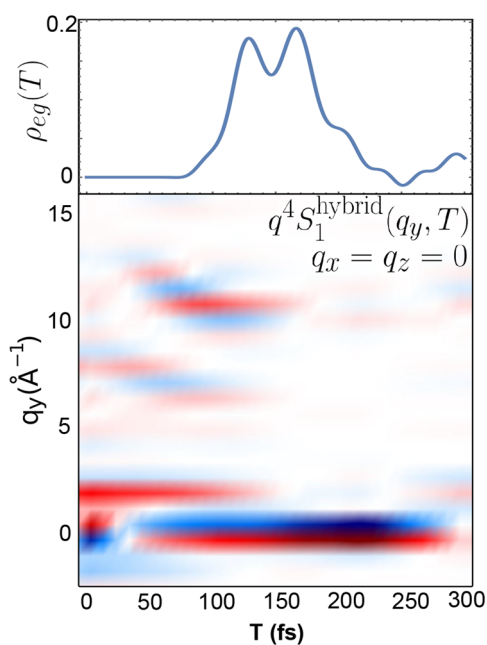


Figure 7. Top: Time evolution of the coherence $\rho_{eg}(T)$. Bottom: Zoom on the hybrid contribution to the signal. The feature at 10 \AA^{-1} appears at 70 fs and disappears at 170 fs, matching with the lifetime of the coherence created at the CoIn.

The UED signal is defined by the integrated rate of change of the electron number $\langle \dot{N}_{k_e} \rangle$ in the detector direction:

$$S_{\text{UED}}(\mathbf{k}_e) = \int dt \langle \dot{N}_{k_e} \rangle \quad (5)$$

where \mathbf{k}_e is the momentum of the observed electron. By perturbatively expanding the expectation value into the

interaction Hamiltonian of the incoming electron beam, eq 4, the expression of the UED signal, eq 1 is obtained.

Closed expressions of the UED signal can be obtained by summing over molecular eigenstates and by separating the charge densities into their electronic and nuclear origins. The resulting contributions are represented by the 12 diagrams depicted in Figure 8.

Wavepacket Simulations. To model azobenzene photoisomerization, we perform exact nuclear wavepacket simulations according to the time-dependent Schrödinger equation

$$i\hbar \frac{\partial}{\partial t} \psi = \hat{H}\psi = [\hat{T}_q + \hat{V}]\psi \quad (6)$$

in the reduced-dimensional space of two reactive coordinates q . In eq 6, ψ is the nuclear wavepacket, and \hat{T}_q and \hat{V} are the kinetic and potential energy operator. As identified in refs 13 and 23, two nuclear coordinates are relevant for the *cis* \rightarrow *trans* photoisomerization. The first one is the reactive carbon–nitrogen–nitrogen–carbon (CNNC) torsion that connects the *cis* and *trans* structures at 0° and $\pm 180^\circ$. The second coordinate is one of the two CNN bending angles between the azo unit and one of the two benzene rings, where the other angle remains fixed at 116° . This symmetry breaking is necessary to reach the minimum conical intersection seam that is located between CNNC = 80° to 110° and CNN = 133° and 147° .

Potential energy surfaces to represent \hat{V} in eq 6 were calculated in ref 23 on the multistate Restricted Active Space Self Consistent Field (RASSCF) and the Second-Order Perturbation Theory Restricted Active Space (RASPT2) levels of theory with the MOLCAS program³² and using the ANO-L-VDZP basis set.³³ An active space of 18 electrons in 16 orbitals was employed, including all π and π^* orbitals and the two nitrogen lone pairs.

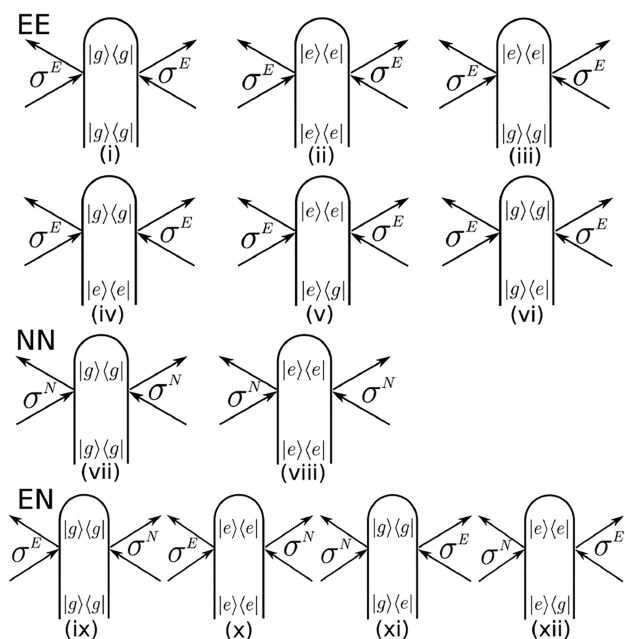


Figure 8. Loop diagrams representing the UED signal. The first two rows are purely electronic contributions (also measured by tr-XRD). The third row corresponds to scattering off the nuclear part of the charge density. The bottom row represents the hybrid electronic/nuclear scattering.

Using this, the nuclear grid was discretized with 600 grid points in CNNC and 256 in CNN. After impulsive excitation of the vibrational ground state wave function to S_1 , the Chebychev propagation scheme³⁴ was used to numerically integrate eq 6 with a time step of 0.05 fs. Impulsive excitation by 100% is an approximation and usually not achieved in experiment. In the case of fractional excitation, a constant background of elastic ground state scattering from the cis geometry will be present in the signal, which qualitatively does not influence the structure of the nuclear and electronic scattering terms. The kinetic energy operator \hat{T}_q in eq 6 is set up according to the G-Matrix formalism³⁵ in $M = 2$ reactive coordinates r and s as described in refs 36 and 37:

$$\hat{T}_q \simeq -\frac{\hbar^2}{2m} \sum_{r=1}^M \sum_{s=1}^M \frac{\partial}{\partial q_r} \left[G_{rs} \frac{\partial}{\partial q_s} \right] \quad (7)$$

with the G-Matrix computed via its inverse elements

$$(G^{-1})_{rs} = \sum_{i=1}^{3N} m_i \frac{\partial x_i}{\partial q_r} \frac{\partial x_i}{\partial q_s} \quad (8)$$

In the S_1 state, periodic boundary conditions are employed along the CNNC torsion. A Butterworth filter³⁸ was used to absorb the nuclear wavepacket at the borders in the CNN direction, a process that acts as a loss channel and that is not further captured by our Hamiltonian. In S_0 the filter was also employed at 0° and 360° of torsion. This absorbs the parts of the wavepacket that have reached the product minimum.

Electronic and Nuclear Densities. The state and transition densities $\sigma_{ij}(q, R)$ were evaluated in 2° increments in CNNC between 0° and 360° torsion and CNN bending between 80° and 180° (a total of 9180 grid points). They were evaluated from the state specific charge density matrices P_{rs}^{ij} according to

$$\sigma_{E,ij}(\mathbf{q}, \mathbf{R}) = \int d\mathbf{r} e^{-i\mathbf{q}\cdot\mathbf{r}} \sum_{rs} P_{rs}^{ij}(\mathbf{R}) \phi_r^*(\mathbf{r}, \mathbf{R}) \phi_s(\mathbf{r}, \mathbf{R}) \quad (9)$$

using the basis set of atomic orbitals $\phi_r(\mathbf{r})$. There are a total of 246 $\phi_r(\mathbf{r})$ orbitals for azobenzene in the ANO-L-VDZP basis (14 for each nitrogen and carbon and 5 for each hydrogen). All 96 electrons of azobenzene contribute to the diagonal state densities σ_{ii} , while the transition density consists of one electron located in the nitrogen lone pairs (see Figure 1b).

The nuclear charge density was calculated as

$$\sigma_{N,ij}(\mathbf{q}) = \delta_{ij} \int d\mathbf{r} e^{-i\mathbf{q}\cdot\mathbf{r}} \int d\mathbf{R} \chi_i^*(\mathbf{R}) \chi_j(\mathbf{R}) \sum_a eZ_a \delta(\mathbf{r} - \mathbf{R}_a(\mathbf{R})) \quad (10)$$

where $\mathbf{R}_a^p(\mathbf{R})$ is a function that returns the coordinates of the atom a in real space at a given reduced coordinate \mathbf{R} , and $\chi_i(\mathbf{R})$ is the nuclear wavepacket of the state i PES.

Our simulations account for symmetric torsion, that is, CNNC angles between $+$ and -180° . This corresponds to mirroring the azobenzene along the molecular plane and results in the complex real-space densities displayed Figure 3, as both positive and negative torsion values contribute equally.

AUTHOR INFORMATION

Corresponding Authors

Jérémy R. Rouxel – Department of Chemistry and Physics & Astronomy, University of California, Irvine, California 92697-2025, United States; Univ Lyon, UJM-Saint-Etienne, CNRS, Graduate School Optics Institute, Laboratoire Hubert Curien UMR 5516, Saint-Etienne F-42023, France;

orcid.org/0000-0003-3438-6370;

Email: jeremy.rouxel@univ-st-etienne.fr

Daniel Keefer – Department of Chemistry and Physics & Astronomy, University of California, Irvine, California 92697-2025, United States; orcid.org/0000-0001-5941-5567; Email: dkeefe@uci.edu

Shaul Mukamel – Department of Chemistry and Physics & Astronomy, University of California, Irvine, California 92697-2025, United States; orcid.org/0000-0002-6015-3135; Email: smukamel@uci.edu

Authors

Flavia Aleotti – Dipartimento di Chimica Industriale, Università degli Studi di Bologna, Bologna I-40136, Italy

Artur Nenov – Dipartimento di Chimica Industriale, Università degli Studi di Bologna, Bologna I-40136, Italy;

orcid.org/0000-0003-3071-5341

Marco Garavelli – Dipartimento di Chimica Industriale, Università degli Studi di Bologna, Bologna I-40136, Italy;

orcid.org/0000-0002-0796-289X

Complete contact information is available at: <https://pubs.acs.org/10.1021/acs.jctc.1c00792>

Notes

The authors declare no competing financial interest.

ACKNOWLEDGMENTS

We gratefully acknowledge support from the Chemical Sciences, Geosciences, and Bio-Sciences Division, Office of Basic Energy Sciences (OBES), Office of Science, U.S. Department of Energy, through award No. DE-SC0019484. D.K. gratefully acknowledges support from the Alexander von

Humboldt foundation through the Feodor Lynen program. J.R.R. was supported by the LABEX MANUTECH-SISE (ANR-10-LABX-0075) of Université de Lyon, within the program "Investissements d'Avenir" (ANR-11-IDEX-0007) operated by the French National Research Agency (ANR) and by the Fédération de Recherche André Marie Ampère (FRAMA). We thank Markus Kowalewski for providing his QDng quantum dynamics code.

REFERENCES

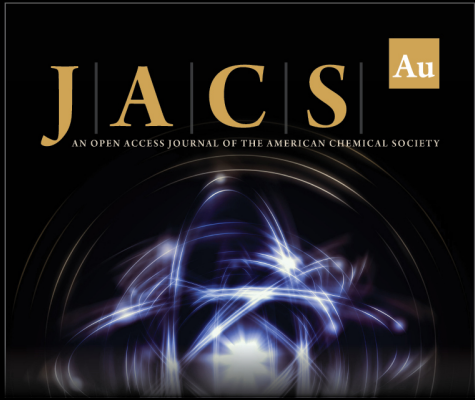
- (1) Zewail, A. H. 4D ultrafast electron diffraction, crystallography, and microscopy. *Annu. Rev. Phys. Chem.* **2006**, *57*, 65–103.
- (2) Miller, R. D. Mapping atomic motions with ultrabright electrons: The chemists' Gedanken experiment enters the lab frame. *Annu. Rev. Phys. Chem.* **2014**, *65*, 583–604.
- (3) Sciaaini, G.; Miller, R. D. Femtosecond electron diffraction: heralding the era of atomically resolved dynamics. *Rep. Prog. Phys.* **2011**, *74*, 096101.
- (4) Siwick, B. J.; Dwyer, J. R.; Jordan, R. E.; Miller, R. D. Ultrafast electron optics: Propagation dynamics of femtosecond electron packets. *J. Appl. Phys.* **2002**, *92*, 1643–1648.
- (5) Ischenko, A. A.; Weber, P. M.; Miller, R. D. Capturing chemistry in action with electrons: realization of atomically resolved reaction dynamics. *Chem. Rev.* **2017**, *117*, 11066–11124.
- (6) Kim, H. W.; Vinokurov, N. A.; Baek, I. H.; Oang, K. Y.; Kim, M. H.; Kim, Y. C.; Jang, K.-H.; Lee, K.; Park, S. H.; Park, S.; et al. Towards jitter-free ultrafast electron diffraction technology. *Nat. Photonics* **2020**, *14*, 245–249.
- (7) Chatelain, R. P.; Morrison, V. R.; Klarenaar, B. L.; Siwick, B. J. Coherent and incoherent electron-phonon coupling in graphite observed with radio-frequency compressed ultrafast electron diffraction. *Physical review letters* **2014**, *113*, 235502.
- (8) Yang, J.; Zhu, X.; Wolf, T. J.; Li, Z.; Nunes, J. P. F.; Coffee, R.; Cryan, J. P.; Gühr, M.; Hegazy, K.; Heinz, T. F.; et al. Imaging CF3I conical intersection and photodissociation dynamics with ultrafast electron diffraction. *Science* **2018**, *361*, 64–67.
- (9) Wolf, T. J.; Sanchez, D.; Yang, J.; Parrish, R.; Nunes, J.; Centurion, M.; Coffee, R.; Cryan, J.; Gühr, M.; Hegazy, K.; et al. The photochemical ring-opening of 1, 3-cyclohexadiene imaged by ultrafast electron diffraction. *Nature Chem.* **2019**, *11*, 504–509.
- (10) Yang, J.; Zhu, X.; Nunes, J. P. F.; Jimmy, K. Y.; Parrish, R. M.; Wolf, T. J.; Centurion, M.; Gühr, M.; Li, R.; Liu, Y.; et al. Simultaneous observation of nuclear and electronic dynamics by ultrafast electron diffraction. *Science* **2020**, *368*, 885–889.
- (11) Parrish, R. M.; Martínez, T. J. Ab Initio Computation of Rotationally-Averaged Pump-Probe X-ray and Electron Diffraction Signals. *J. Chem. Theory Comput.* **2019**, *15*, 1523–1537.
- (12) Srinivasan, R.; Lobastov, V. A.; Ruan, C.-Y.; Zewail, A. H. Ultrafast electron diffraction (UED) a new development for the 4D determination of transient molecular structures. *Helvetica chimica acta* **2003**, *86*, 1761–1799.
- (13) Keefer, D.; Aleotti, F.; Rouxel, J. R.; Segatta, F.; Gu, B.; Nenov, A.; Garavelli, M.; Mukamel, S. Imaging conical intersection dynamics during azobenzene photoisomerization by ultrafast X-ray diffraction. *Proc. Natl. Acad. Sci. U.S.A.* **2021**, *118*, e2022037118.
- (14) Rouxel, J. R.; Keefer, D.; Mukamel, S. Signatures of electronic and nuclear coherences in ultrafast molecular x-ray and electron diffraction. *Structural Dynamics* **2021**, *8*, 014101.
- (15) Bennett, K.; Kowalewski, M.; Rouxel, J. R.; Mukamel, S. Monitoring molecular nonadiabatic dynamics with femtosecond X-ray diffraction. *Proc. Natl. Acad. Sci. U. S. A.* **2018**, *115*, 6538–6547.
- (16) Rouxel, J. R.; Kowalewski, M.; Bennett, K.; Mukamel, S. X-ray sum frequency diffraction for direct imaging of ultrafast electron dynamics. *Physical review letters* **2018**, *120*, 243902.
- (17) Kowalewski, M.; Bennett, K.; Mukamel, S. Monitoring nonadiabatic avoided crossing dynamics in molecules by ultrafast X-ray diffraction. *Structural Dynamics* **2017**, *4*, 054101.
- (18) Goulet-Hanssens, A.; Eisenreich, F.; Hecht, S. Enlightening materials with photoswitches. *Adv. Mater.* **2020**, *32*, 1905966.
- (19) Kienzler, M. A.; Reiner, A.; Trautman, E.; Yoo, S.; Trauner, D.; Isacoff, E. Y. A red-shifted, fast-relaxing azobenzene photoswitch for visible light control of an ionotropic glutamate receptor. *J. Am. Chem. Soc.* **2013**, *135*, 17683–17686.
- (20) Bozovic, O.; Jankovic, B.; Hamm, P. Using azobenzene photocontrol to set proteins in motion. *Nat Rev Chem* **2021**, DOI: 10.1038/s41570-021-00338-6.
- (21) Nägele, T.; Hoche, R.; Zinth, W.; Wachtveitl, J. Femtosecond photoisomerization of cis-azobenzene. *Chem. Phys. Lett.* **1997**, *272*, 489–495.
- (22) Fujino, T.; Arzhantsev, S. Y.; Tahara, T. Femtosecond/Picosecond Time-Resolved Spectroscopy of trans-Azobenzene: Isomerization Mechanism Following $S_2(\pi\pi^*)\leftarrow S_0$ Photoexcitation. *Bull. Chem. Soc. Jpn.* **2002**, *75*, 1031–1040.
- (23) Aleotti, F.; Soprani, L.; Nenov, A.; Berardi, R.; Arcioni, A.; Zannoni, C.; Garavelli, M. Multidimensional Potential Energy Surfaces Resolved at the RASPT2 Level for Accurate Photoinduced Isomerization Dynamics of Azobenzene. *J. Chem. Theory Comput.* **2019**, *15*, 6813–6823.
- (24) Quick, M.; Dobryakov, A.; Gerecke, M.; Richter, C.; Berndt, F.; Ioffe, I.; Granovsky, A.; Mahrwald, R.; Ernsting, N.; Kovalenko, S. Photoisomerization dynamics and pathways of trans-and cis-azobenzene in solution from broadband femtosecond spectroscopies and calculations. *J. Phys. Chem. B* **2014**, *118*, 8756–8771.
- (25) Aquilante, F.; Autschbach, J.; Carlson, R. K.; Chibotaru, L. F.; Delcey, M. G.; De Vico, L.; Fdez. Galván, I.; Ferré, N.; Frutos, L. M.; Gagliardi, L. Molcas 8: New capabilities for multiconfigurational quantum chemical calculations across the periodic table. *J. Comput. Chem.* **2016**, *37*, 506.
- (26) Kovacs, G. N.; Colletier, J.-P.; Grünbein, M. L.; Yang, Y.; Stensitzki, T.; Batyuk, A.; Carbajo, S.; Doak, R. B.; Ehrenberg, D.; Foucar, L.; et al. Three-dimensional view of ultrafast dynamics in photoexcited bacteriorhodopsin. *Nat. Commun.* **2019**, *10*, 1–17.
- (27) Yong, H.; Zotev, N.; Ruddock, J. M.; Stankus, B.; Simmermacher, M.; Carrascosa, A. M.; Du, W.; Goff, N.; Chang, Y.; Bellshaw, D.; et al. Observation of the molecular response to light upon photoexcitation. *Nat. Commun.* **2020**, *11*, 1–6.
- (28) Ma, L.; Yong, H.; Geiser, J. D.; Moreno Carrascosa, A.; Goff, N.; Weber, P. M. Ultrafast x-ray and electron scattering of free molecules: A comparative evaluation. *Structural Dynamics* **2020**, *7*, 034102.
- (29) Zheng, J.-C.; Zhu, Y.; Wu, L.; Davenport, J. W. On the sensitivity of electron and X-ray scattering factors to valence charge distributions. *Journal of applied crystallography* **2005**, *38*, 648–656.
- (30) Liu, Y.; Horton, S. L.; Yang, J.; Nunes, J. P. F.; Shen, X.; Wolf, T. J.; Forbes, R.; Cheng, C.; Moore, B.; Centurion, M.; et al. Spectroscopic and structural probing of excited-state molecular dynamics with time-resolved photoelectron spectroscopy and ultrafast electron diffraction. *Physical Review X* **2020**, *10*, 021016.
- (31) de Kock, M.; Azim, S.; Kassier, G.; Miller, R. Determining the radial distribution function of water using electron scattering: A key to solution phase chemistry. *J. Chem. Phys.* **2020**, *153*, 194504.
- (32) Aquilante, F.; Autschbach, J.; Carlson, R. K.; Chibotaru, L. F.; Delcey, M. G.; De Vico, L.; Fdez. Galván, I.; Ferré, N.; Frutos, L. M.; Gagliardi, L.; et al. Molcas8: New capabilities for multiconfigurational quantum chemical calculations across the periodic table. *J. Comput. Chem.* **2016**, *37*, 506–541.
- (33) Widmark, P.-O.; Malmqvist, P.-Å.; Roos, B. O. Density matrix averaged atomic natural orbital (ANO) basis sets for correlated molecular wave functions. *Theoretica chimica acta* **1990**, *77*, 291–306.
- (34) Tal-Ezer, H.; Kosloff, R. An accurate and efficient scheme for propagating the time dependent Schrödinger equation. *J. Chem. Phys.* **1984**, *81*, 3967–3971.
- (35) Berens, P. H.; Wilson, K. R. Molecular dynamics and spectra. I. Diatomic rotation and vibration. *J. Chem. Phys.* **1981**, *74*, 4872–4882.
- (36) Thallmair, S.; Roos, M. K.; de Vivie-Riedle, R. Design of specially adapted reactive coordinates to economically compute

potential and kinetic energy operators including geometry relaxation.


J. Chem. Phys. **2016**, *144*, 234104.

(37) Reiter, S.; Keefer, D.; Vivie-Riedle, R. *Quantum Chemistry and Dynamics of Excited States*; Wiley, 2020; pp 355–381.


(38) Butterworth, S. On the Theory of Filter Amplifiers. *Experimental Wireless and the Wireless Engineer* **1930**, *7*, 536–541.




JACS Au
AN OPEN ACCESS JOURNAL OF THE AMERICAN CHEMICAL SOCIETY



Editor-in-Chief
Prof. Christopher W. Jones
Georgia Institute of Technology, USA

Open for Submissions 

pubs.acs.org/jacsau  ACS Publications
Most Trusted. Most Cited. Most Read.